Judd-Ofelt and quantum cutting analysis of Eu3+ or Pr3+ doped β-NaGdF4 nanorods obtained by rapid coprecipitation method

Y. Cheroura, Z. Smara, A. Potdevin, D. Boyer, A. Chafa, O. Ziane, Rachid Mahiou

Judd-Ofelt and quantum cutting analysis of Eu^{3+} or Pr^{3+} doped β-$NaGdF_4$ nanorods obtained by rapid coprecipitation method

Y. Cheroura[1, 2], Z. Smara[1, 3], A. Potdevin[1,], D. Boyer[1], A. Chafa[3], O. Ziane[2], R. Mahiou[1,*]*

[1]Université Clermont Auvergne, CNRS, SIGMA Clermont, Institut de Chimie de Clermont-Ferrand, F-63000 Clermont-Ferrand, France

[2]Laboratoire d'Electronique Quantique, Faculté de Physique, USTHB, El-Alia Bab-Ezzouar, 16111 Alger, Algérie

[3] Laboratoire des Sciences Nucléaires et Interaction Rayonnement Matière, Faculté de Physique, USTHB, El-Alia Bab-Ezzouar, 16111 Alger, Algérie

Abstract

Pure hexagonal β-$NaGdF_4$ and Eu^{3+} or Pr^{3+}-doped β-$NaGdF_4$ nanocrystals in shape of nanorods of ~140 nm of length have been synthesized using a simple and rapid coprecipitation method. XRD analysis evidenced pure single phases exhibiting characteristic luminescence of Eu^{3+} or Pr^{3+} ions when excited under UV or blue radiations. Samples gave rise to intense orange-red emission and quite white emission in the case of respectively Eu^{3+} or Pr^{3+} doped samples. Optical properties are discussed in the frame of Judd-Ofelt theory and considering that an energy transfer occurs between active ions. Notably it was found that the quantum-cutting by a two-step energy transfer from Gd^{3+} to Eu^{3+} can improve the red emission of Eu^{3+} ions under near-VUV excitation. Such quantum-cutting mechanism has been also considered in the case of Pr^{3+} doped β-$NaGdF_4$. However, the efficiency of both processes in comparison with literature suggest that only one part of the energy in the excited states within Gd^{3+} can be transferred to Eu^{3+} for its red emission. In the case of Pr^{3+} ions, the energy is more probably released through the self-trapped exciton emission certainly due to the lack of resonant VUV excitation.

Keywords: Nanorods, fluorides, luminescence, Judd-Ofelt theory

1. Introduction

The fabrication of nano-to micro-scale inorganic structures has attracted great interest as a result of their novel properties and their potential applications in various fields e.g. color displays, solid-state lasers, medicine and Light Emitting Diodes (LEDs) or in specific screens for enhancing solar cells efficiency.[1] In most cases, the as-explored materials are based on the use of lanthanide ions which exhibit efficient luminescence under VUV, UV or IR excitations leading to strong conversion of the excitation wavelength in the range of the desired luminescence in the UV-Visible or IR wavelength range.

To date, Ln^{3+}doped fluorides have been extensively investigated and proved to be the ideal host candidates for producing high up and down conversion luminescence efficiency.[2, 3] $NaGdF_4$ is a member of the $NaREF_4$ family (RE=rare earth), it crystallizes in two phases, cubic α-$NaGdF_4$ and hexagonal β-$NaGdF_4$.[4] Special conditions are required to obtain pure β-$NaREF_4$ nanoparticles (NPs) which exhibits better luminescent properties and thermodynamic stability.[5] Hexagonal β-$NaGdF_4$ phase has a low effective phonon energy of about 350 cm^{-1}, which reduces the probability of non-radiative decay by multiphonon relaxation and thereby enhances the luminescence compared to the cubic phase.[6] Different papers have reported the synthesis of pure hexagonal phases. β-$NaGdF_4$ NPs are mainly prepared by the following methods: high temperature solvothermal or hydrothermal methods or thermal decomposition process[7]. Using solvothermal method, P. Lei *et al.*[8] achieved the synthesis of hexagonal phase β-$NaGdF_4$ using ethylene glycol as solvent at 200°C, for 7h. The synthesis of colloidal β-$NaGdF_4$ NPs was also performed *via* thermal decomposition of fluoride precursors of lanthanide ions. The method was described by J. Ryu *et al.*[9] and E. Hemmer *et al.*[10]. In the first step, the lanthanide trifluoroacetate precursor was prepared at 80°C for 12 h, then sodium trifluoroacetate was added to the flask; octadecene was used as a solvent with oleic acid or oleylamine as surfactants. The solution was maintained at 310°C for 60 min under stirring and argon flow. β-$NaGdF_4$

nanocrystals were prepared as well by N. Martin *et al.* [11] from solution by a co-precipitation method. This method allows a good control of the morphology and homogeneity of the obtained materials and efficiently reduces oxygen contamination but it requires a temperature between 300 and 780°C under SF_6+Ar (10%) atmosphere. Banski *et al.*[12] prepared β-$NaGdF_4$ nanocrystals using trioctylphosphine oxide (TOPO) as a surfactant using a two-step co-thermolysis method at 120°C under vacuum for 30 minutes. Then the growth temperature was increased to 350°C for 1 hour. These methods are cumbersome, because high temperature and/or long reaction time are often needed to obtain the desired β-$NaGdF_4$ NPs in the pure hexagonal form, moreover high amounts of surfactants are used to control the morphology and the size distribution of the NPs. To overcome these drawbacks, several simple synthetic ways have been developed last years. Recently, Gao *et al.*[13] published an easy aqueous synthesis strategy using chlorides and NH_4F as well as β-cyclodextrin as precursors. They had to heat at 60°C during 40 min to obtain β-$NaGdF_4$ nanorods. Tessitore *et al.*[6, 14] used ethylene glycol as a solvent and obtained β-$NaGdF_4$ nanocrystals (2-3 nm) from rare-earth acetates after 24h at room temperature. On the other hand, several papers[15, 16] have reported the synthesis of β-$NaBiF_4$ NPs at room temperature, basing their work on Lei *et al.*'s [17].

In the present work, we report an easy, cost-effective and low energy-consumption strategy to synthesize β-$NaGdF_4$ NPs using a process, based on coprecipitation method, similar to that reported by Lei *et al.*'s [17]. Several synthesis parameters have been optimized to achieve well-crystallized of both undoped and Eu^{3+}- or Pr^{3+}-doped β-$NaGdF_4$ NPs. Simple chemical precursors were involved and the required synthesis time was reduced at 1 hour at only 150°C. Firstly, structural and morphological properties of as-synthesized NPs were studied by means of X-Ray diffraction (XRD), Transmission Electronic Microscopy (TEM) and InfraRed (IR) spectroscopy.

In the second part of our work, the optical properties of Eu^{3+} or Pr^{3+}ions doped β-$NaGdF_4$ NPs were investigated. Such ions are well-known to give rise to visible luminescence, notably in the red range for Eu^{3+} and simultaneously in the blue, green and red ranges for Pr^{3+} leading to quasi white emission. These nanophosphors present the interest to be easily integrable in several optical devices.

To perform these studies, photoluminescence and lifetime measurements were analyzed as a function of the $Eu^{3+}$and Pr^{3+} contents. They are discussed in the frame of energy transfer mechanisms occurring between the active ions. In addition, the Judd-Ofelt [18] analysis based on the recorded emission spectra of Eu^{3+} and Pr^{3+} ions was performed, which allowed calculating radiative and non-radiative transition probabilities, decay lifetimes, and Judd-Ofelt intensity parameters of the luminescence of $Eu^{3+}$and Pr^{3+} doped β-$NaGdF_4$ nanoparticles. Moreover, in $LiGdF_4$:Eu^{3+} [19] and β-$NaGdF_4$:Eu^{3+} [20] systems, a visible quantum cutting with efficiency higher than 100 % have been obtained through the $^6G_J \rightarrow {}^6P_J$ (Gd^{3+}) and $^7F_J \rightarrow {}^5D_0$ (Eu^{3+}) cross-relaxation energy transfer from Gd^{3+} to Eu^{3+}. To investigate whether or not this two-step energy transfer for the couple Gd^{3+}-Eu^{3+} occurs in β-$NaGdF_4$ NPs, emission spectra upon excitation in several Gd^{3+} energy levels were recorded. It is well-known that an energy transfer from Pr^{3+} to Gd^{3+} can occur when the fluoride matrix or the 4f5d bands of Pr^{3+} are excited. [21, 22] However, the near VUV excitation provided by our experimental set-up has allowed observing an emission related to Self-Trapped Emission (STE) in β-$NaGdF_4$: Pr^{3+} NPs indicating that possible quantum cutting can take place in such material by triggering the luminescence of Pr^{3+} in the VUV range.

2. Experimental section

2.1. Materials

Analytical grade gadolinium nitrate hexahydrate ($Gd(NO_3)_3.6H_2O$, 99.9%), sodium nitrate ($NaNO_3$, 99.5%) and ethylene glycol (EG) ($C_2H_2O_2$, 99.8%) were purchased from Acros Organics. Ammonium fluoride (NH_4F, 95%) was obtained from Prolabo (VWR) and europium

nitrate pentahydrate ($Eu(NO_3)_3.5H_2O$, 99.9%), praseodymium nitrate hexahydrate ($Pr(NO_3)_3.6H_2O$, 99.9%) from Sigma-Aldrich. All the above chemicals were used directly without further purification.

2.2. Nanopowder synthesis

The β-$NaGdF_4$ NPs were synthesized using a coprecipitation method as depicted in **Figure 1**. In a typical synthesis route, a solution of EG (10 ml) containing $Gd(NO_3)_3.6H_2O$ (1mmol) and $NaNO_3$ (3 mmol) is added to a solution of EG (20 ml) containing NH_4F (6mmol). The resulting mixture is subsequently heated to different reaction temperatures (25, 50, 100,150 °C), and held for different reaction times (30, 45, 60 min) under vigorous stirring. The detailed experimental parameters including the reacting temperature and reaction time are listed later in Table 1. After cooling to RT, the β-$NaGdF_4$ NPs are collected through centrifugation and washed several times with ethanol, distilled water and then dried at 80°C for 24h.

Eu^{3+} and Pr^{3+} -doped NPs were synthesized following the same procedure, using the optimal parameters of temperature and reaction time defined on undoped matrix, and using Eu nitrate pentahydrate ($Eu(NO_3)_3.5H_2O$, 99.9%) or Pr^{3+}nitrate hexahydrate ($Pr(NO_3)_3.5H_2O$, 99.9%) in variable amounts as rare-earth precursors. The total lanthanide ions (Gd+Ln, Ln = Eu or Pr) concentration was kept constant (1 mmol) in all experiments, whereas the doping rate (molar ratio Ln/Gd with Ln=Eu or Pr) varies from 1% to 30 % and from 0.1% to 1% respectively in order to investigate the effect of this parameter on the luminescent properties.

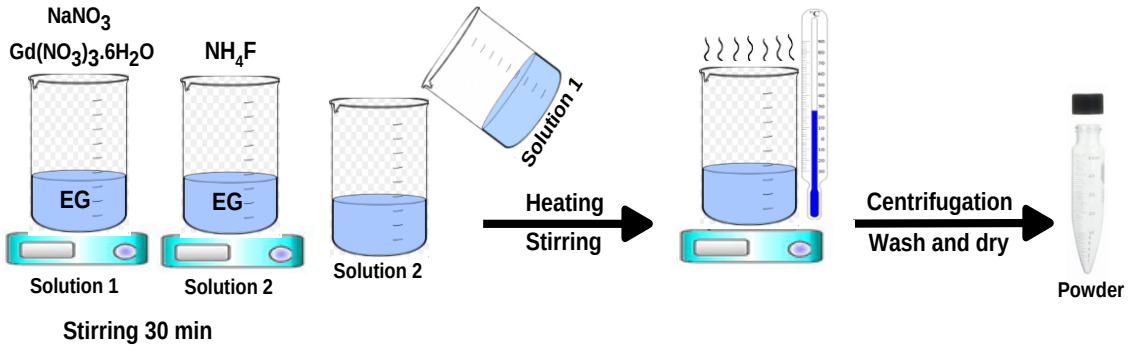

Figure 1 : Schematic illustration of the synthesis procedure of β-$NaGdF_4$ nanoparticles

2.3. Technical Characterizations

Structural and morphological characterizations

The X-ray diffraction (XRD) analysis were performed at room temperature with a commercial X'Pert Pro Philips diffractometer equipped with a back monochromator using the Bragg- Brentano configuration and the Cu-Kα radiation (λ=1.5406 Å) over 2θ range from 10° to 90° with step size of 0.02°. All the data were processed by XPert High Score plus Software using databases (unit cell parameters, peak identification).

Particles size measurements were carried out using Dynamic Light Scattering; their distributions were obtained using the Zetasizer Nano ZS, Malvern, U.K. Instrument.

Transmission Electronic Microscopy (TEM) images were recorded on a Hitachi H-7650 microscope at the Centre Imagerie Cellulaire Santé (CICS) of Clermont-Ferrand.

Fourier transform infrared spectra were performed from polycrystalline samples with a Thermo Electron (Nicolet 5700-FTIR model) spectrometer equipped with a diamond micro-Attenuated Total Reflection (ATR) accessory and working with OMNIC software. Spectra were recorded from 4000 to 400 cm^{-1} at a spectral resolution of 4 cm^{-1} and 400 scans were accumulated for improving the signal/noise ratio.

Luminescence analysis

The optical properties were investigated by recording the photoluminescence spectra with a Jobin-Yvon set-up consisting of a Xenon lamp operating at 400 W and two monochromators (Triax 550 and Triax 180) combined with a cryogenically cold charge coupled device (CCD) camera (Jobin-Yvon Symphony LN2 series) for emission spectra and with a Hamamatsu 980 photomultiplicator for excitation ones.

Quantum yields (QY) efficiencies were assessed using C9920−02G PL-QY measurement system from Hamamatsu. The set-up consisted of a 150 W monochromatized Xe lamp, an integrating sphere (Spectralon coating, ∅= 3.3 in.) and a high sensibility CCD camera.

Photoluminescence excitation (PLE) spectra were obtained by exciting the NPs from 250 to 500 nm with 5 nm increment and measuring their absolute QY. The absolute PL QYs were calculated by combining the internal QY values with the absorption coefficient (also measured by the apparatus).

Luminescence decays were recorded using a second-harmonic generation beam delivered by a pulsed Nd:YAG OPO-Ekspla NT342A laser (3-5 ns pulse duration, 10 Hz, 5 cm^{-1} line width , 0.3 mJ in the UV). The emitted photons were detected at right angle from the excitation and analyzed through Edinburgh FLS980 spectrometer (Czerny-Turner monochromator, 300 mm focal length, 1200 groove mm^{-1} grating and minimum band-pass of 0.1 nm) equipped with Hamamatsu R928P PMT (200-870 nm range).

3. Results and discussion

3.1. Structural and Morphological study of undoped $NaGdF_4$

To study the effect of reaction time and synthesis temperature on the crystalline structure, XRD patterns were recorded from samples prepared with different reaction times going from 30 to 120 min, and with synthesis temperatures varying from Room Temperature (RT) to 150°C, are illustrated in

Figure 2**.** The detailed parameters and crystalline phase of the as-obtained samples are listed in **Table 1**.

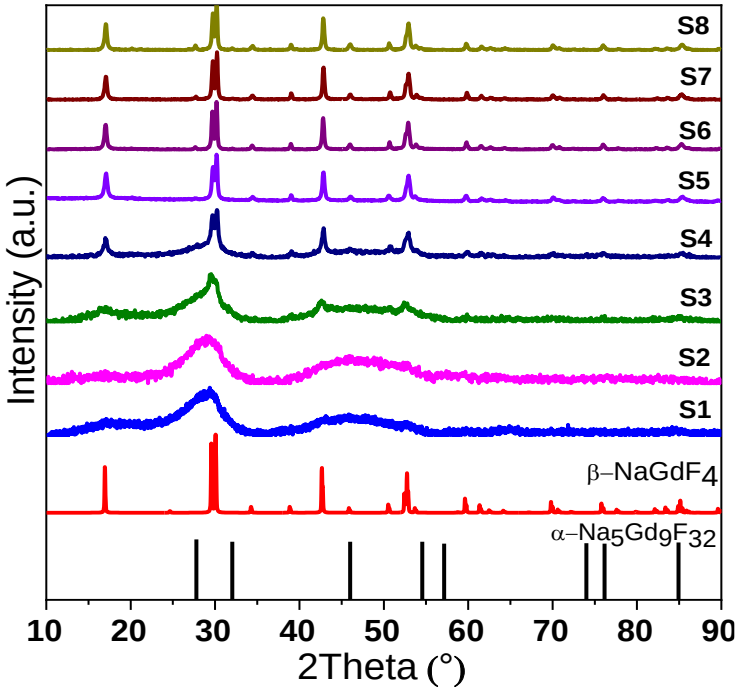

Figure 2 : XRD patterns of the samples prepared with different conditions of temperature and time reaction

Table 1 : Detailed experimental parameters and crystal phase of the as-obtained samples

Sample	Reaction time (min)	Reaction temperature (°C)	Crystal phase
S1	30	RT	Amorphous
S2	60	RT	Amorphous
S3	60	100	Amorphous
S4	45	150	Amorphous
S5	60	150	β-$NaGdF_4$
S6	75	150	β-$NaGdF_4$+α-$Na_5Gd_9F_{32}$
S7	90	150	β-$NaGdF_4$ +α-$Na_5Gd_9F_{32}$
S8	120	150	β-$NaGdF_4$+α-$Na_5Gd_9F_{32}$

These results indicate that, at room temperature, the reaction time has no influence on the crystal phase of the samples: they remain amorphous till 60 min since no diffraction peak is observed (Figure 2 S1 and S2).

It can be also seen that the variation of the reaction temperature highly affects the crystalline phase of the resultant samples. The beginning of crystallization is observed for the sample obtained at 100°C for 60 min (Figure 2 S3). When the reaction temperature is increased to 150°C for 45 min (Figure 2 S4), diffraction peaks are more apparent and the resultant product is more crystallized. With the reaction temperature of 150°C for 60 min (Figure 2 S5), all the diffraction peaks can be readily indexed as the hexagonal β-$NaGdF_4$, agreeing well with the data reported in the JCPDS standard file (n°027-0699) and no byproduct can be observed. Thus, the β-$NaGdF_4$ can be synthesized at 150°C for 60 min *via* this facile strategy. It is worth noting that, to our knowledge, it is the first report on the hexagonal phase β-$NaGdF_4$ NPs synthesized at such a low heating temperature at ambient pressure. For reaction time longer than 60 min at 150°C, a small amount of α-$Na_5Gd_9F_{32}$ is observed and becomes more and more present with increasing the synthesis time. This phase has received more and more attention in recent years. [23, 24] In particular, Xu *et al.* worked on the synthesis of β-$NaGdF_4$ or $Na_5Gd_9F_{32}$ using hydrothermal synthesis (8h at 160°C). In the absence of ethylene-glycol, used to modify diffusion behavior of the reactants, their synthesis resulted in a mixture of β-$NaGdF_4$ and $Na_5Gd_9F_{32}$. Basing on their study, the presence of $Na_5Gd_9F_{32}$ may be the result of a slower diffusion rate of Gd^{3+} ions compared to other species. Indeed, if the reaction time is sufficiently long, more Gd^{3+} ions can react with F^- and Na^+ ions to give birth to $Na_5Gd_9F_{32}$ phase following the equation: [23, 24]

$$9\ Gd^{3+} + 32\ F^- + 5\ Na^+ \rightarrow Na_5Gd_9F_{32}$$

TEM study has been carried out to characterize β-$NaGdF_4$ morphology. On the TEM image corresponding to S5 (**Figure 3**a), one can clearly observe nanorods with a shape similar to those obtained by Gao *et al.*[13] but much smaller. Indeed, according to the size distribution diagrams reported in Figure 3b (for the length), the average length of β-$NaGdF_4$ nanorods is around 140 ±20 nm whereas their width is around 60±4 nm.

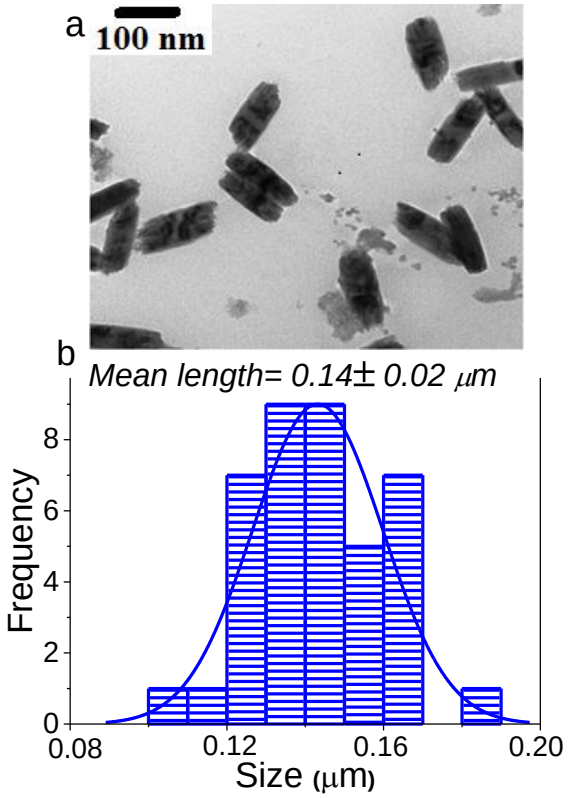

Figure 3 : (a)TEM image and (b) size distribution of β-$NaGdF_4$ nanocrystals.

The hydrodynamic diameter measured by DLS in an aqueous particles suspension is about 200 nm. This value is only slightly larger than the mean particle size estimated from the TEM micrographs of the sample and confirmed the absence of particle aggregation in the aqueous suspension.

The presence of ethylene glycol (EG) ligands at the surface of β-$NaGdF_4$ nanocrystals has been evidenced by FTIR as shown on the FTIR spectrum of as prepared β-$NaGdF_4$ nanorods (S5) (**Figure 4**a). A comparison with IR spectra of liquid-EG (Figure 4b) is used to tentatively attribute IR features. The peaks corresponding to physically absorbed water or ethylene glycol appear at around 3244 cm^{-1} and 1640 cm^{-1} for stretching and bending modes respectively[25]. The bands observed at 2900, 1424, 1346 and 830 cm^{-1} are ascribed to the stretching vibrations, wagging vibrations and rocking mode of CH_2- groups. The absorption peaks appearing at 1090 and 1060cm^{-1} are related to the C-O and C-C stretching vibrations arising from EG adsorbed

on the surface of β-$NaGdF_4$ NPs.[26] Basing on these spectra, EG seems to act as a capping-agent in this synthesis route. This behavior is probably responsible for the anisotropic growth of β-$NaGdF_4$ nanocrystals, as it has already been evidenced by Zhao and his co-workers.[26]

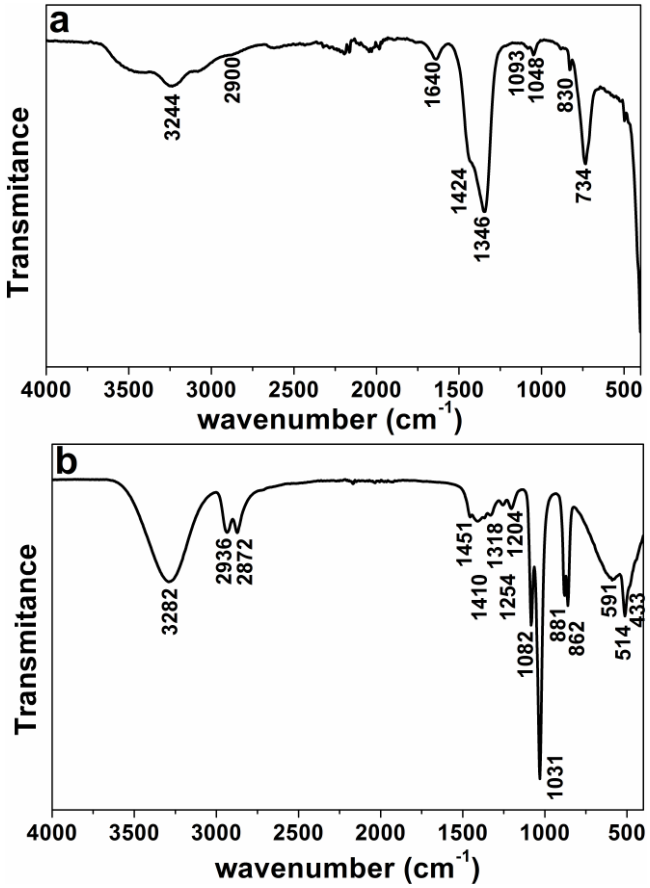

Figure 4 : FTIR spectra of (a) β-$NaGdF_4$ nanorods and (b) liquid EG

3.2. Synthesis and Characterization of β-$NaGdF_4$:Ln^{3+} Nanoparticles (Ln^{3+} = Eu^{3+}or Pr^{3+}).

The syntheses are carried out using the method previously described and optimized from the undoped material (sample S5). Gadolinium and europium or praseodymium amounts were adjusted to achieve different doping rates (molar ratios): 1%, 5%, 10%, 20% and 30% for Eu^{3+} ions and 0.1%, 0.5% and 1.0% for Pr^{3+}ones. The differences in doping rates used for each dopant are due to the fact that concentration quenching for Pr^{3+}doped materials is known to appear at much lower doping levels than in the case of Eu^{3+} doping.[27, 28] TEM images (**Figure 5**) have evidenced that the shape and size of the undoped NPs are reproduced for all doped samples irrespective of nature of doping ions and doping rates. The XRD patterns of the doped

β-$NaGdF_4$:Eu^{3+} and β-$NaGdF_4$:Pr^{3+} particles are very similar to the one of the undoped material as shown in **Figure 6**a and **Figure 7**a. In both cases, diffraction peaks are slightly shifted toward lower 2theta values (Figure 6b and Figure 7b), which indicates an increase in the unit cell size of the doped materials compared to the undoped NPs. Such increase confirms that Gd^{3+} (effective ionic radius in nine-fold coordination:1.247Å)[29]: ions have been successfully substituted by the larger radius size doping ions (Eu^{3+} -1.26 Å or Pr^{3+} -1.319 Å).

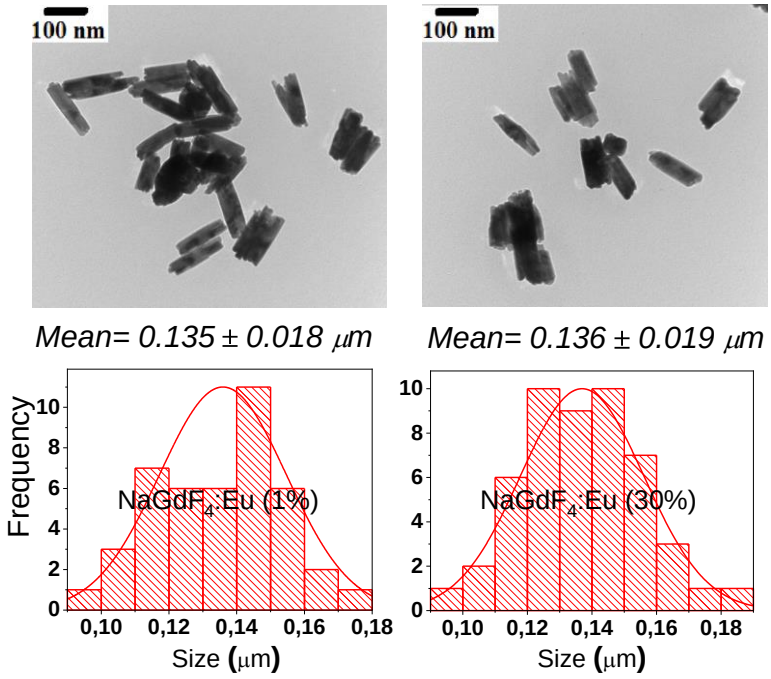

Figure 5 : TEM images and particle size distribution of the β-$NaGdF_4$:Eu^{3+} (1%, 30%) nanoparticles

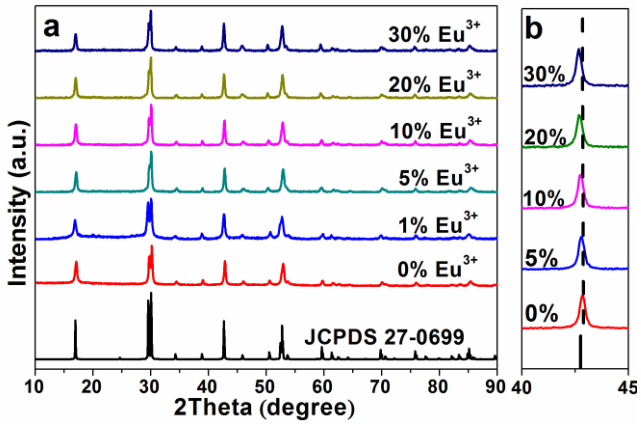

Figure 6 : XRD patterns (a) and magnified XRD patterns (b) of β-$NaGd_{1-x}F_4$:x% Eu^{3+} NPs (x= 0, 1, 5, 10, 20, 30)

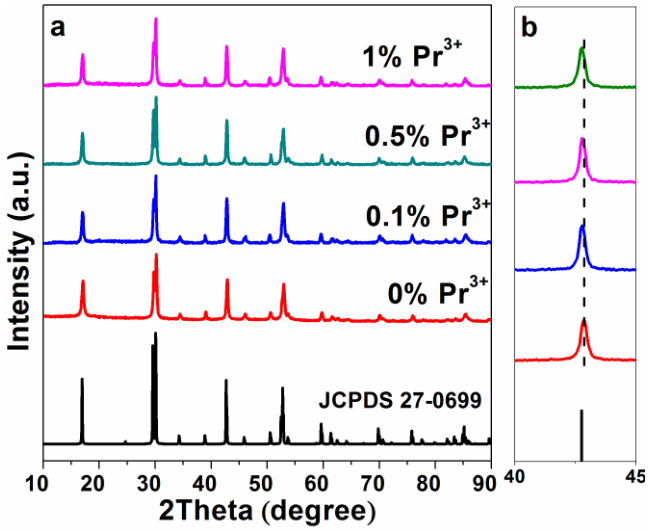

Figure 7 : XRD patterns (a) and magnified XRD patterns (b) of β-$NaGd_{1-x}F_4$:x% Pr^{3+} NPs (x = 0.1, 0.5, 1)

To confirm effective replacement of Gd^{3+} by Eu^{3+} and Pr^{3+} in the crystal structure of β-$NaGdF_4$ and the corresponding formation of the β-$NaGd_{1-x}Eu_xF_4$ and β-$NaGd_{1-x}Pr_xF_4$ NPs , the XRD patterns of the doped particles were analyzed by X'Pert High Score plus Software to obtain the corresponding unit cell parameters (**Table 2**). The obtained values have been plotted in **Figure 8**, where a linear increase of the unit cell volume can be observed with increasing doping rate in both cases. The observed behavior satisfies Vegard's law [30] and indicates that Eu^{3+} and Pr^{3+}ions are substituting Gd^{3+} in β-$NaGdF_4$ crystal structure.

Table 2 : Refined unit cell parameters of β-$NaGdF_4$:Eu^{3+} and β-$NaGdF_4$:Pr^{3+} samples

Compound	a, b (Å)	c (Å)	Volume (Å ^{3})
β-$NaGdF_4$	6.018(2)	3.609(1)	113.2(1)
β-$NaGdF_4$:Eu^{3+}(5%)	6.017(2)	6.612(2)	113.2(1)
β-$NaGdF_4$:Eu^{3+}(10%)	6.018(2)	6.617(2)	113.4(1)
β-$NaGdF_4$:Eu^{3+}(20%)	6.025(2)	6.610 (2)	113.6(1)
β-$NaGdF_4$:Eu^{3+}(30%)	6.033(2)	6.610 (2)	113.8(1)
β-$NaGdF_4$:Pr^{3+}(0.5%)	6.027(2)	3.606(1)	113.4(1)

β-$NaGdF_4$:Pr^{3+}(1%)	6.020(2)	3.621(2)	113.6(1)

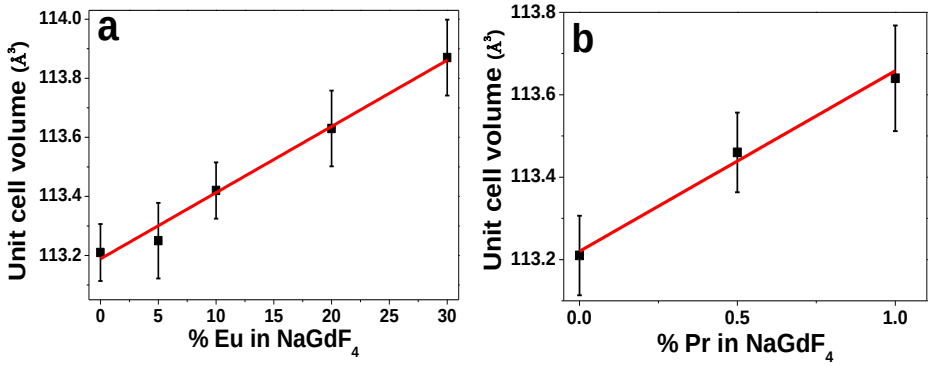

Figure 8 : Evolution of unit cell volumes of β-$NaGdF_4$: Eu^{3+} (a) and β-$NaGdF_4$: Pr^{3+} (b) samples versus Eu and Pr content (mol%)

3.3. Luminescence properties of the β-$NaGdF_4$:Ln (Ln = Eu^{3+}or Pr^{3+}) Nanoparticles.

3.3.1: Steady state

PhotoLuminescence Quantum yield Excitation (PLQE) spectra of $NaGdF_4$:x% Eu^{3+} (x=1,5,10,20 and 30%) NPs were recorded at room temperature as a function of excitation wavelength from 250 nm to 500 nm with a 3 nm increment (**Figure 9**), monitoring the overall Eu^{3+} emission arising from the $^5D_0$ level of Eu^{3+} ions. The internal quantum yield efficiencies correspond to the ratio between the emitted and the absorbed photons while the absolute quantum yield efficiencies are obtained taking into account the absorption coefficient. Maxima of quantum yield efficiencies are observed for all samples under an excitation wavelength peaking at 275 nm, corresponding to the $^8S_{7/2} \rightarrow {}^6I_{7/2}$ absorption transition of Gd^{3+}, and at 395 nm corresponding to the $^7F_0 \rightarrow {}^5L_6$ absorption transition of Eu^{3+}. The observation of the $^8S_{7/2} \rightarrow {}^6P_J, {}^6I_{7/2}$ transitions confirms an intense $Gd^{3+} \rightarrow Eu^{3+}$ energy transfer. Under excitation at 275 nm, both the UV emission of Gd^{3+} at ~ 311 nm and the orange-red emissions of Eu^{3+} at ~ 590-620 nm are observed, and the emission intensity of Gd^{3+} decreases when Eu^{3+} concentration increases but does not completely disappear even though the *x* value reaches 0.30. The internal and absolute quantum yields obtained at room temperature for an excitation wavelength of 395 nm are reported in **Table 3**. The best value is obtained for β-$NaGdF_4$:20%

Eu^{3+} sample (**Figure 10**) for which the absolute photoluminescence quantum yield (PLQY) was found to be of ~ 11%.

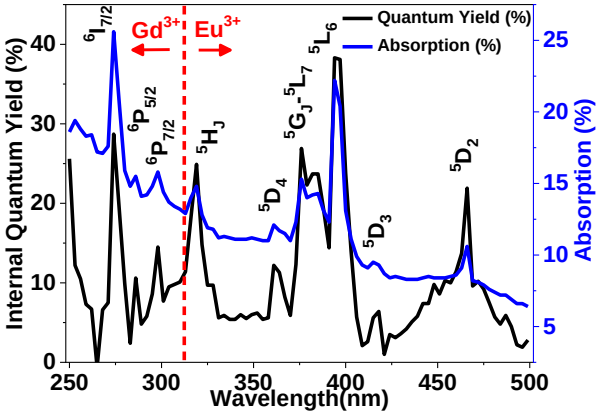

Figure 9 : Internal quantum yield and absorption coefficient of β-NaGdF4:20% Eu^{3+}.

The internal efficiency ε_{in} and the external quantum efficiency ε_{ex} were determined by

$$\varepsilon_{in} = \frac{N_{em}}{N_{abs}} \qquad [1]$$

$$\varepsilon_{ex} = \frac{N_{em}}{N_{ex}} = \varepsilon_{in}\left(\frac{N_{abs}}{N_{ex}}\right) \qquad [2]$$

where N_{em} corresponds to the number of photons for the sample's emission light, N_{abs} corresponds to the number of photons that are absorbed by the sample, and N_{ex} corresponds to the number of photons for the excitation light from a Xe light source. N_{em} was calculated from the area of the emission peak for the sample. N_{abs} was obtained by subtracting the area of the reflection peak at the excitation wavelength for the sample from that for a sample free standard holder quartz cell, whereas N_{ex} was calculated from the area of the reflection peak at the excitation wavelength for a sample free standard holder quartz cell. The two values are obtained automatically by our absolute PL quantum yield measurement system, equipped with an integrating sphere Spectralon coated (Hamamatsu QY- C9920−02G) with an uncertainty of 5% and repeatability better than 2%.

Table 3 : Quantum efficiencies for β-$NaGdF_4$:x% Eu^{3+} (x=1, 5, 10, 20 and 30%) for λ_{exc} = 95 nm

Sample x%	Internal quantum yield %	Absorption coefficient	Absolute quantum yield %
1	17	0.12	2
5	27	0.22	6
10	21	0.34	7
20	43	0.26	11
30	28	0.27	7

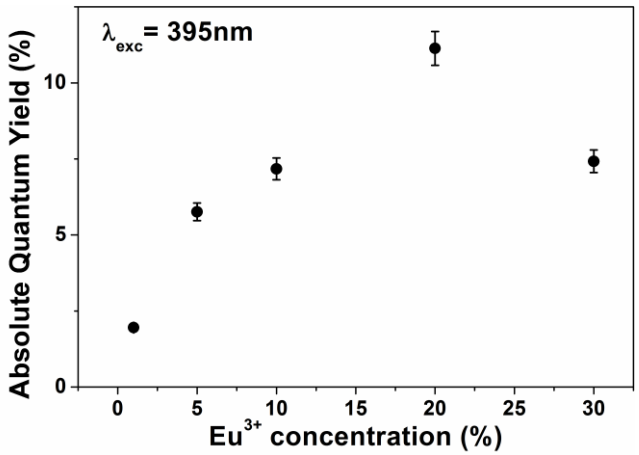

Figure 10 : Absolute Quantum yield of β-$NaGdF_4$:x% Eu^{3+} (x= 1, 5, 10, 20 and 30 %) upon λ_{exc}= 395 nm

Figure 11 shows a photoluminescence (PL) spectrum of β-$NaGdF_4$:Eu^{3+}1% nanocrystal recorded at room temperature upon Gd^{3+}-$^8S_{7/2}\rightarrow{}^6I_{7/2}$ excitation at 275nm. The emission spectrum exhibits four characteristic bands peaking at around 592, 618, 650, and 696 nm that correspond to the $^5D_0\rightarrow{}^7F_{J'}$ (J'= 1, 2, 3, and 4) spin forbidden f-f electronic transitions of the Eu^{3+} ions. In addition, transitions from higher ^5D_J (J = 1–2) levels to the $^7F_{J'}$ manifold in the explored wavelength range are observed. The $^5D_0\rightarrow{}^7F_1$ transition is the parity-allowed magnetic dipole transition ($\Delta J' = 1$) and its intensity does not vary with the nature of the host.[31] On the contrary, the $^5D_0\rightarrow{}^7F_2$ electric dipole transition ($\Delta J' = 2$), which is in this case the most

dominant, is very sensitive to the local environment around Eu^{3+}, and its intensity depends on the symmetry of the crystal field around the europium ions.[32]

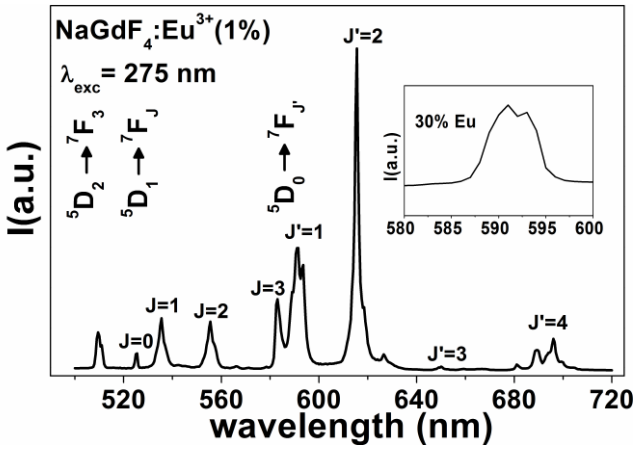

Figure 11 : Emission spectrum of β-$NaGdF_4$:Eu^{3+} (1 mol %) recorded at RT upon Gd^{3+}-$^8S_{7/2}\rightarrow{}^6I_{7/2}$ excitation at 275 nm. The inset shows the emission spectrum of β-$NaGdF_4$:Eu^{3+}(30 mol%) in the vicinity of $^5D_0\rightarrow{}^7F_{0,1}$ transitions.

In the hexagonal β-$NaLnF_4$ phase (Ln= Y, Gd, Eu, - matrices belonging to space group $P\bar{6}$), the $^5D_0\rightarrow{}^7F_0$ transition is not allowed since 0–0 transition is forbidden by the selection rule $J = 0 \rightarrow J' = 0$. The inset of Figure 11 shows clearly that the $^5D_0\rightarrow{}^7F_0$ transition is not recorded in the β-$NaGdF_4$:Eu^{3+} (30 mol%) for which the emissions arising from the upper ^5D_J (J=1-3) are quenched at this Eu^{3+} ion concentration. Lower energy transitions, $^5D_0\rightarrow{}^7F_3$ and $^5D_0\rightarrow{}^7F_4$, are also clearly visible. In our case, for the pure hexagonal β-$NaGdF_4$:Eu^{3+}, an asymmetric intensity ratio $I(^5D_0\rightarrow{}^7F_2)/I(^5D_0\rightarrow{}^7F_1)$ of the electric dipole to magnetic dipole transitions of ~ 1.6 is determined. This value is widely different (smaller) than those mentioned in literature for β-$NaGdF_4$ host [20, 33] which is around ~ 2.6. This ratio serves as an effective spectroscopic probe of the site symmetry in which Eu^{3+} ions are situated. High values indicate lower symmetry and the absence of a center of inversion for the Eu^{3+}site, low values its presence.[20]

For better understanding and quantification, the f–f emission transition intensities of Eu^{3+} in β-$NaGdF_4$ nanocrystals are analyzed by means of the Judd–Ofelt (JO) model. We have

calculated the asymmetry parameter Ω_2 which gives information on the intensity and nature of the hypersensitive transition of the Eu^{3+}ions (for more details see **Supporting Information**).

Table 4 : calculated asymmetry parameter $\boldsymbol{\Omega_2}$ for this work and in literature.

	This work	[Ref [20]]	[Ref [33]]	[Ref [34]]
$\Omega_2 \times 10^{-20} cm^2$	2.33	13.94	11.60	2.33

The lower $\Omega_2(2.33 \times 10^{-20} cm^2)$ value calculated for the pure hexagonal phase β-$NaGdF_4$ synthesized in this work, compared to that reported in Ghosh and co-workers[20, 33] **(**Table 4), suggests that the Eu^{3+} ions reside here in a highly symmetric environment. In fact, for hexagonal β-$NaGdF_4$ crystal (space group $P\bar{6}$), low local site symmetries for Eu^{3+} ions are possible; these sites are situated at (0,0,0), the 1a site, and at (2/3,1/3,1/2), the 1f site. The 1a site is fully occupied by RE (Gd, Eu) ions, whereas Na^+ and RE^{3+} (Gd^{3+}, Eu^{3+}) ions are randomly distributed among the 1f sites. The point site symmetry of the 1a and 1f sites is commonly described as C_{3h}[35] or D_{3h} [36]. Such symmetry sites can be lowered by local deformation induced by lower crystallinity in the case of NPs in regard to the bulk crystal. However, the absence in our case of the $^5D_0 \rightarrow {}^7F_0$ transition is an indication that the symmetry is higher than the common C_s, C_n or C_{nv} local symmetries found for Eu^{3+} embedded in NPs. More precisely, such transition is observed in the case of β-$NaGdF_4$: Eu^{3+} nanocrystals as reported in Ref [[37]]. In that case, the more comprehensive explanation can arise from the fact that small part of the Eu^{3+} doping ions enter in the 2h site of Na^+ [38] for which the local symmetry is C_3; which allows observation of the $^5D_0 \rightarrow {}^7F_0$ transition. More simply, we can consider that the notable difference in asymmetry parameter Ω_2 can be explained by the doping-induced breakdown of crystallographic site symmetry.[39] For Eu^{3+}-doped β-$NaGdF_4$ crystals synthesized using Ghosh and co-workers' methods,[20, 33] when Eu^{3+} ions are doped in the Gd lattice of β-$NaGdF_4$, the local site symmetry of Eu^{3+} was lowered from C_{3h} or D_{3h} to lower symmetries such as C_s, C_3, or C_1. On the contrary,

using our method and the method reported by Ref [34], the local site symmetry of Eu^{3+} ions remains C_{3h} or D_{3h}. Since the numbering of the Stark components of the $^5D_0 \rightarrow {}^7F_J$ transitions is not possible, due the nanoscopic form of the samples, we can't state on the nature of the site symmetry. Such considerations indicate that the site symmetry of Eu^{3+} ions in the NPs is dependent on the synthesis method used for their preparation.

For the Gd^{3+} ions, an emission in the UV is recorded for all the samples as unresolved broad band peaking at around ~ 311 nm corresponding to the $^6P_{7/2} \rightarrow {}^8S_{7/2}$ fluorescence (**Figure 12**). Such observation confirms the nanoscale character of the NPs.

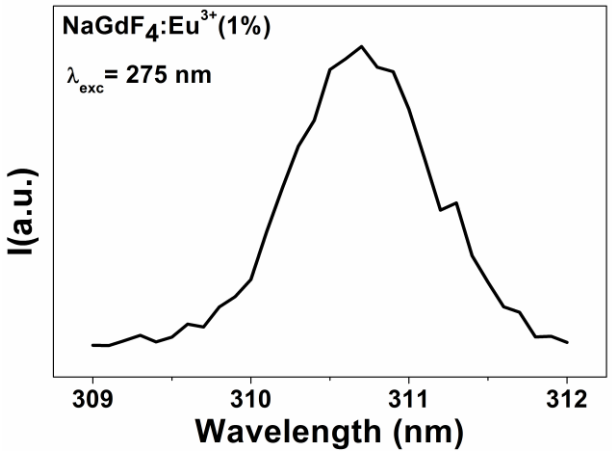

Figure 12 : UV Emission spectrum of $^6P_{7/2} \rightarrow {}^8S_{7/2}$ transition of Gd^{3+} in β-$NaGdF_4$:Eu^{3+}(1 mol%) recorded at RT upon Gd^{3+}-$^8S_{7/2} \rightarrow {}^6I_{7/2}$ excitation at 275nm.

The emission spectra of β-$NaGdF_4$: Pr^{3+} at room temperature under the excitation of 444 nm ($^3H_4 \rightarrow {}^3P_2$) was depicted in **Figure 13**. All emissions having maxima at 469, 484, 523, 539, 591, 603, 641 and 653 nm are mainly attributed to the transitions from $^3P_0$ or $^3P_1$ to ^3H_J (J=4-6) and to $^3F_2$ and $^3F_3$. However, we have considered that an emission from the $^1D_2$ level in the vicinity of $^3P_1 \rightarrow {}^3H_6$ and $^3P_0 \rightarrow {}^3H_4$ is also present as recently reported by J.J Velázquez *et al.* [28] in β-$NaGdF_4$: Pr^{3+}nanocrystals. We will discuss such possibility in the next part of the paper related to the luminescence dynamics. In addition, the excitation spectra monitoring the blue or red emission, which are not reported here, presents only the absorption bands from $^3H_4$ ground state to the $^3P_2$, $^3P_1$-$^1I_6$ and $^3P_0$ excited states in agreement with a previous work[28]. Notably, no

absorption in the UV wavelength range was recorded, confirming the absence of a possible $Gd^{3+} \rightarrow Pr^{3+}$ energy transfer. Occurrence of emission originating from the $^3P_1$ state has been already reported for β-$NaYF_4$: Pr^{3+} and the feeding of this level from the upper excited states of Pr^{3+} is explained by a two-ion interaction.[40]

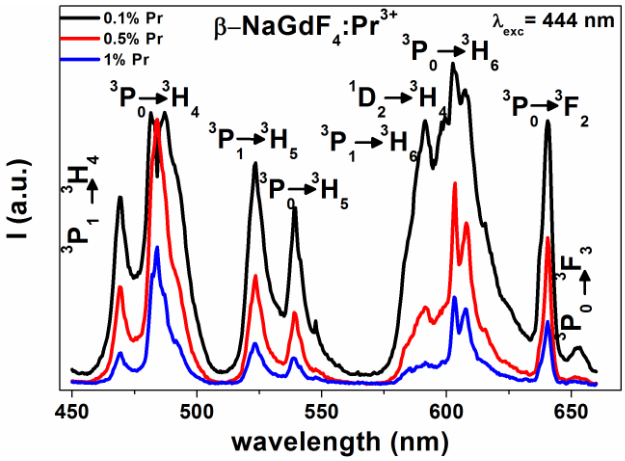

Figure 13 : Emission spectra of β-$NaGdF_4$:Pr^{3+} (0.1, 0.5, 1 mol%) recorded at RT upon Pr^{3+}- $^3H_4 \rightarrow {}^3P_2$ excitation at 444 nm.

3.3.2: Luminescence dynamics and Judd-Ofelt analysis

Gd^{3+}-Eu^{3+} pair has been extensively studied as efficient energy transfer ion couple.[41] The luminescence decay of the $^6P_{7/2} \rightarrow {}^8S_{7/2}$ transition in the undoped β-$NaGdF_4$ sample is exponential with time constant of ~ 37μs. **Figure 14** shows the Eu^{3+} ion concentration dependence of the Gd^{3+}: $^6P_{7/2} \rightarrow {}^8S_{7/2}$ luminescence decay curves under excitation at 275nm ($^8S_{7/2} \rightarrow {}^6I_{7/2}$) at room temperature.

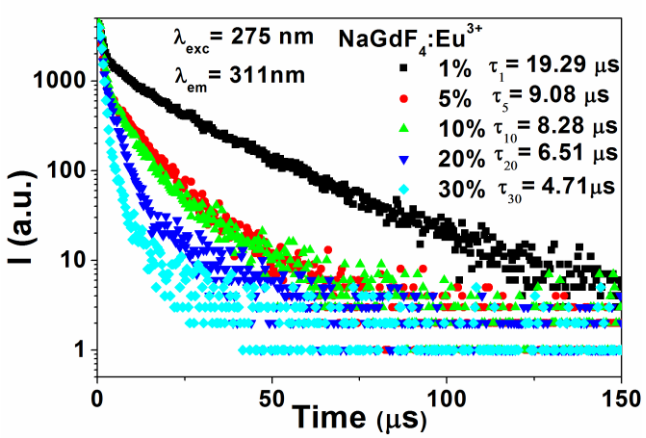

Figure 14 : Decay curves of $^6P_{7/2} \rightarrow {}^8S_{7/2}$ transition of Gd^{3+} in β-$NaGdF_4$:xEu^{3+}(x= 1, 5, 10, 20, 30 mol%)

All the decay curves are non-exponential and present no rise time indicating fast de-excitation from the Gd^{3+}- $^6I_{7/2}$ to the Gd^{3+}- $^6P_{7/2}$ level. They become faster and faster with the increase in Eu^{3+} concentration. Such observation is another confirmation of the Gd^{3+} to Eu^{3+} energy transfer. Generally, for such energy transfer, the luminescence decays of the donor (in occurrence Gd^{3+}), when they diverge from a single exponential, are parametrized in the frame of exchange or dipole or multipole electric interactions between the donor (Gd^{3+}) and the acceptor (Eu^{3+}).[42, 43] Such consideration is not the purpose of our paper and we haven't tried to fit the decays. For this reason, we have estimated the average fluorescent lifetimes (τ_m) using the following equation:[44]

$$\tau_m = \frac{\int_0^\infty I(t)\, t\, dt}{\int_0^\infty I(t)\, dt} \simeq \frac{\int_0^{tmax} I(t)\, t\, dt}{\int_0^{tmax} I(t)\, dt} \quad (3)$$

The derived results are reported on Figure 14 and spread from 19.3 µs for Gd^{3+} in β-$NaGdF_4$: 1% Eu^{3+} to 4.7 µs for $^6P_{7/2} \rightarrow {}^8S_{7/2}$ transition of Gd^{3+} in β-$NaGdF_4$: 30% Eu^{3+}. However, these values are notably lower than the time constant found for $^6P_{7/2} \rightarrow {}^8S_{7/2}$ emission of Gd^3 in bulk β-$NaGdF_4$ where it reaches 1.4 ms.[45]

The effect of Eu^{3+} concentration on decay times of Eu^{3+}-$^5D_0 \rightarrow {}^7F_2$ (615 nm) transition under 275 nm excitation is shown in **Figure 15**. The luminescence decay time curves are well fitted with two exponential components, one in the initial rise time and another in the decaying part

at long time. Exactly same decays in the shape and in the time constant values are recorded when the excitation stands at 395 nm in the $^7F_0 \rightarrow {}^5L_6$ absorption transition of Eu^{3+}.Through build-up process, the energy absorbed in $^6I_{7/2}(Gd^{3+})$ is transferred to upper excited states than $^5L_6$ of Eu^{3+} from which non radiative relaxation ensure the population of the ^5D_J emitting levels. This build-up is obviously influenced by the Eu^{3+} concentration. It becomes faster with increasing Eu^{3+} concentration and disappears for the high Eu^{3+} concentrations, starting from 10%. The tail of the decays is mono exponential until 20% mol content of Eu^{3+} and diverges slowly from single exponential for β-$NaGdF_4$: 30% Eu^{3+}. In that case, the decays are fitted by bi-exponential function. The values derived from the fits are reported on Figure 15. The rise time is estimated at ~ 2 ms for the 1% doped sample. This value is higher than that estimated for $^6P_{7/2} \rightarrow {}^8S_{7/2}$ transition of Gd^{3+} (19.3μs), confirming that the recorded rise time is more characteristic of non-radiative relaxations occurring from the upper excited states of Eu^{3+} ions to their first excited state $^5D_0$. Such consideration is supported by the fact that emissions from, for example the $^5D_{1,2}$ levels of Eu^{3+}, are observed under excitation in the $^6I_{7/2}$ (Gd^{3+}) or $^5L_6$ (Eu^{3+}) excited levels (Figure 11).

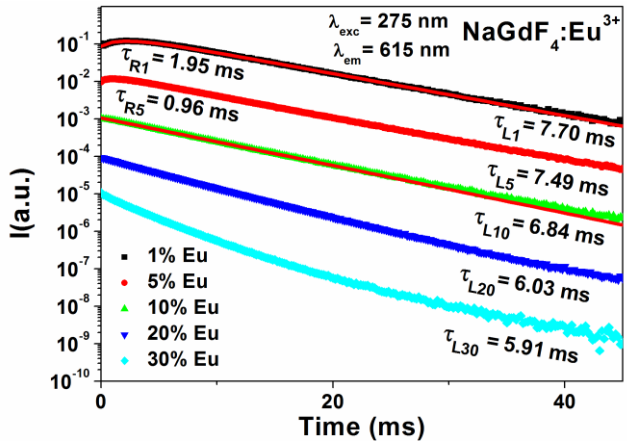

Figure 15 : Decay curves of $^5D_0 \rightarrow {}^7F_2$ transition of Eu^{3+} in β-$NaGdF_4$:xEu^{3+}(x= 1, 5, 10, 20, 30 mol%) under excitation at 275 nm at room temperature.

In the tail of the decays, the values of the time constants spread over 7.7 ms in β-$NaGdF_4$: 1% Eu^{3+} to 5.9 ms in β-$NaGdF_4$: 30% Eu^{3+}. These values are close to that reported for β-

$NaGdF_4$: 2% Eu^{3+} nanorods for which the measured lifetime is 9.17 ms under excitation at 272 nm ($^8S_{7/2} \rightarrow {}^6I_{7/2}$). [20] However, in that report, the nanorods are mixed materials containing both α and β-$NaGdF_4$ phases and also exhibit the $^5D_0 \rightarrow {}^7F_0$ in addition of a high asymmetry parameter Ω_2 of 13.94 (Table 4).

JO intensity parameters are essential indicators in judging radiative potential of RE ions in different hosts, which are usually derived from absorption spectrum. Effective absorption measurement is very difficult for powdered phosphors but some reports exist in the literature [46-48]. Indeed, owing to the special energy level structure of Eu^{3+}, they can be calculated from the suitably calibrated emission spectra to correct for the detector response, grating efficiency and other optical elements which may be related to the experimental set-up and taking into account the total area of each $^5D_0 \rightarrow {}^7F_J$ transitions. The several steps of the procedure are reported in supplementary information **SI1** for Eu^{3+}-doped samples.

The calculated JO parameters values are presented in **Table 5** with the values of radiative and non-radiative emission probabilities and decay lifetimes. The theoretical JO parameters, radiative and non-radiative rates, decay lifetime calculated from the Judd–Ofelt analysis of luminescence spectra well agree with the results reported by Bednarkiewicz and co-workers.[34]

Table 5: $\boldsymbol{\Omega_{2,4}}$ JO parameters, radiative transition rates ($\boldsymbol{A_r}$), nonradiative rates ($\boldsymbol{A_{nr}}$), calculated ($\boldsymbol{\tau_{rad}}$) and ($\boldsymbol{\tau_{exp}}$) experimental decay life time $^5D_0$ for Eu^{3+} in β-$NaGdF_4$ sample.

	$\Omega_2 \times 10^{-20} cm^2$	$\Omega_4 \times 10^{-20} cm^2$	$A_r(s^{-1})$	$A_{nr}(s^{-1})$	$\tau_{rad}(ms)$	$\tau_{exp}(ms)$
[Ref [33]]	2.33	2.62	133.8	-22.5	7.47	9.02
This work	2.33	0.99	133.3	-3.4	7.51	7.70

The calculated radiative lifetime value of the $^5D_0$ state of Eu^{3+} for the pure hexagonal β-$NaGdF_4$:Eu^{3+} sample is 7.51 ms and nicely match with that measured in β-$NaGdF_4$: 1%Eu^{3+} (7.7ms). The ratio of the experimental lifetime to the predicted radiative lifetime is defined as

quantum efficiency (QE = τ_{exp}/τ_{rad}) of the corresponding level. It depends on the considered sample, since the τ_{exp} is modified by the Eu^{3+} amount contained in the material. In our case, the derived QE values are of ~100% for 1 and 5% Eu^{3+} content and of ~ 90%, and ~80% for respectively the 10% Eu^{3+} content and 20 as well as 30% Eu^{3+} content. These values are questionable, because it is necessary to take into account uncertainties on the measured values and on the JO analysis derived values. An estimated uncertainty of 5% for each of these values leads to an overall uncertainty of 10%. The most important information is the QE value of the 20% Eu^{3+} for which the measured absolute (external) quantum yield is of 11% ± 5% is in the order range of the external quantum obtained by correcting the QE from the absorption coefficient (Table 3) which is of 90% x 26% = 23.4% ± 10%.

The luminescence decays of Pr^{3+} ions doped β-$NaGdF_4$,under excitation in the $^3P_2$ excited level at 444 nm ($^3H_4 \rightarrow {}^3P_2$), monitoring the main emissions peaking at 484 and 615 nm (Figure 13), are depicted on **Figure 16** and **Figure 17** respectively.

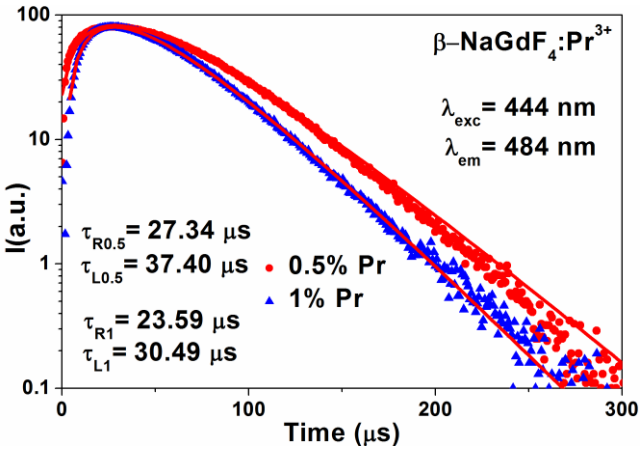

Figure 16 : Decay curves of $^3P_0 \rightarrow {}^3H_4$ transition of Pr^{3+} in β-$NaGdF_4$:xPr^{3+}(x= 0.5, 1 mol%) under excitation at 444 nm at room temperature.

The emission at 484 nm corresponds to the $^3P_0 \rightarrow {}^3H_4$ transition of Pr^{3+} ions. As shown on Figure 13, for the 0.1 % Pr^{3+} doped sample, this emission is very broad and clearly overlap with the $^3P_1 \rightarrow {}^3H_5$ transition. For this reason, the corresponding decay is not depicted on Figure 16. For the two other Pr^{3+} concentrations, the luminescence decays are dominated at short time by

a build-up characteristic of the feeding of the $^3P_0$ level from the upper excited states followed in the tail by an exponential decaying. The values derived from the fits by two exponential function, one in the rise and another in the tail of the decays, are reported on Figure 16. The decaying time constants of the $^3P_0$ level, of ~ 37 and ~ 30 μs for respectively the 0.5% and 1 % doped samples are close to the radiative lifetimes found in β-$NaYF_4$:Pr^{3+}(i.e. 22 μs)[49] or in $LiYF_4$: Pr^{3+} (i.e. 38 μs),[50] but diverge notably from the values reported for β-$NaGdF_4$:Pr^{3+} nanocrystals doped with 0.1% and 0.5% Pr^{3+} which they are of ~ 10 and ~ 6 μs respectively.[20] Such discrepancy can perhaps be explained by the fact that, in ref [20], the β-$NaGdF_4$:Pr^{3+} nanocrystals are synthesized *in-situ* in oxyfluoride glass-ceramics by the melting-quenching method which can induce a large amount of defects at the surface of the nanocrystals inherent to the interface between the glass and the nanocrystals; these defects being responsible for the shorter lifetimes. Figure 17 reports the luminescence decays of the emission peaking in the red at 615 nm. For the 1% doped sample, the shape of the decay is quite similar to that reported for $^3P_0 \rightarrow {}^3H_4$ emission (Figure 16). The only difference resides in the small decrease of the rise time from ~ 24μs to ~ 20μs. For the two other concentrations 0.1 and 0.5%, we do not observe an initial rise time and the decays are non-exponential. They are fitted by a bi-exponential function, the derived time constants of which are reported on Figure 17.

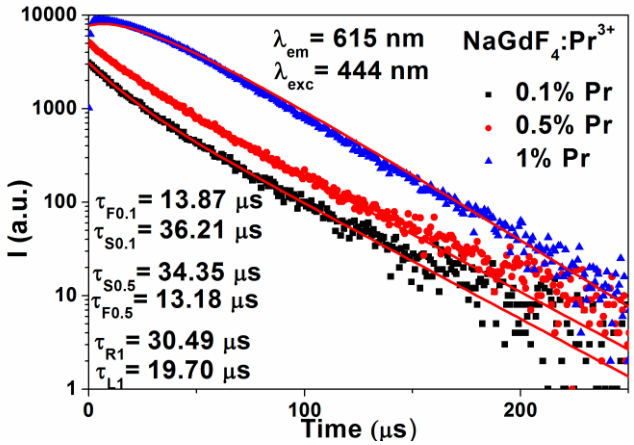

Figure 17 : Decay curves of red emission at 615 nm of Pr^{3+} in β-$NaGdF_4$:xPr^{3+}(x= 0.1, 0.5, 1 mol%) under excitation at 444 nm at room temperature.

The values found in the tail are consistent with the radiative lifetime of the $^3P_0$ level as discussed above. Origin of the short time component of ~ 13-14 μs is puzzling. It can't correspond to the time constant of the luminescence arising from the $^3P_1$ level, since its value can be estimated from the rise time of the decay of $^3P_0 \rightarrow {}^3H_4$ emission which is considered around ~ 23-27μs. Another possibility resides in considering that this slow component can be attributed to the radiative decaying from the $^1D_2$ level to the $^3H_4$ ground state of Pr^{3+} ions. The $^1D_2$ level in this scheme is populated *via* cross-relaxation processes between Pr^{3+} ions such as $^3P_0 \rightarrow {}^3H_6$ and $^3H_4 \rightarrow {}^1D_2$. Such mechanism is concentration-dependent since the $^1D_2$ level exhibit rapid quenching and has already been reported for example in the oxides, like YPO_4:Pr^{3+},[51] in which the intensity ratio between the emissions arising from the $^3P_0$ and $^1D_2$ increases with increasing the Pr^{3+} concentration. Such consideration can perhaps explain satisfactorily why the luminescence decay of the emission peaking at 615 nm for 1 % concentration is more characteristic of the radiative decaying from the $^3P_0$ level. However, the time constant of the $^1D_2$ level in β-$NaYF_4$: 0.1%Pr^{3+} bulk powdered samples that we have prepared by solid-state reaction has been measured around 313 μs at 300 K, which is larger than the one we have measured in the NPs obtained by co-precipitation. In conclusion, some supplementary experiments are needed to state about the possible emission from the $^1D_2$ level of Pr^{3+} ions in β-

$NaGdF_4$: Pr^{3+}. As in the case of Eu^{3+}, we have tried to analyze the JO parameters of Pr^{3+} ions in β-$NaGdF_4$: Pr^{3+} on the basis of the emission spectra, since we had not the possibility to record absorption spectra in the case of powdered samples. The $^3P_0$ excited level, which is not degenerated, can play similar role than the $^5D_0$ level of Eu^{3+} ions. Such procedure has been successfully reported for Pr^{3+}-doped Mg_2SiO_4 nanophosphors.[52] In our case, it is possible then to determine the JO intensity parameters Ω_λ (where λ= 2, 4 6) based on the emission data. For a particular transition, the emission intensity (I) can be considered as proportional to the area under the emission curve for that transition. ~~However, T~~he average transition energies are obtained from emission spectra as an average over the selected transition region. Obtained values were collected and reported in **Table 6**. The steps used for the calculation of the parameters are reported in supplementary information **SI-2**.

Table 6 : Judd-Ofelt intensity parameters ($\boldsymbol{\Omega_2}$, $\boldsymbol{\Omega_4}$, $\boldsymbol{\Omega_6}$) of β-$NaGdF_4$:Pr^{3+} compounds

Pr^{3+} conc. (mol %)	$\Omega_2\ (10^{-20}cm^2)$	$\Omega_4(10^{-20}cm^2)$	$\Omega_6(10^{-20}cm^2)$
0.1	5.25	0.12	0.44
0.5	3.73	0.13	0.31
1	3.85	0.13	0.44

We have no reference for comparison to assess the validity of such a procedure in the case of fluorides. However, all the J-O parameters are quasi-independent of the Pr^{3+}concentration except the Ω_2 parameter which is higher in the case of 0.1% doped sample. This parameter which mainly connects the transitions with ΔJ = 2 can perhaps explain the existence of an efficient energy transfer between $^3P_0$ and $^1D_2$ levels in the 1% doped sample in addition to the radiative relaxation to the $^3F_2$ level. Further experiments are needed to support such a possibility. However, as presented in the case of Eu^{3+}, the quantum efficiency QE can be estimated using an average of τ_{rad} derived from JO analysis of 35 μs and considering that the

experimental τ_{exp} can be estimated from the tail of the decays; the calculated QE values are of ~ 100, 98 and 87% for 0.1, 0.5 and % Pr^{3+} content in the samples.

3.3.3: Quantum cutting

Recently, quantum cutting phenomenon in β-$NaGdF_4$:Eu^{3+}emission of two visible photons per VUV photon absorbed was demonstrated.[31] In order to study this mechanism, emission spectra of pure hexagonal β-$NaGdF_4$:Eu^{3+} are recorded at room temperature upon excitation at 210 nm and upon excitation in the $^6I_{7/2}$ level of Gd^{3+} ions at 275 nm, as shown in **Figure 18**, which reports the emission spectra under both excitation wavelengths for β-$NaGdF_4$: 5%Eu^{3+}. The excitation at 210 nm is the up limit of our experimental set-up which can't stand at 204 nm which corresponds to the $^8S_{7/2}\rightarrow{}^6G_{7/2}$ absorption transition of Gd^{3+} ions. However, we have considered that this excitation wavelength is not so far to be resonant with the $^6G_{7/2}$ excited level of Gd^{3+}, such as suggested by recording the $^8S_{7/2}\rightarrow{}^6P_{7/2}$transition under this excitation (210 nm) with luminescence decay fitting the one reported in Figure 14. Since $^5D_1\rightarrow{}^7F_J$ transitions should be not modified by the quantum cutting effect, their emission intensities are used as a reference to scale both emission spectra.

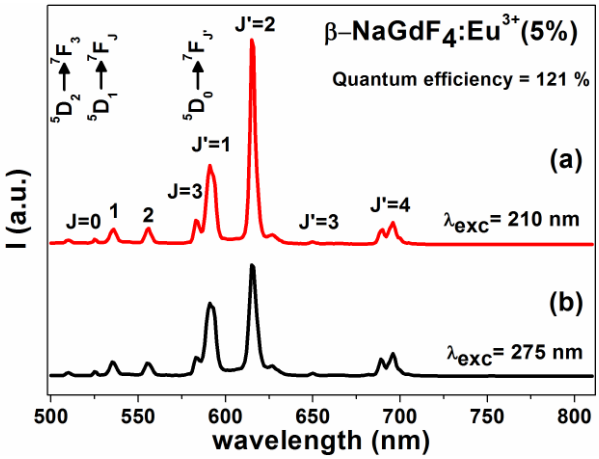

Figure 18 :Emission spectra of β-$NaGdF_4$:Eu^{3+} (5 mol%) recorded at RT upon (a)close to Gd^{3+}-$^8S_{7/2}\rightarrow{}^6G_J$ excitation at 210 nm and upon (b) Gd^{3+}-$^8S_{7/2}\rightarrow{}^6I_{7/2}$ excitation at 275 nm. Both spectra are scaled on the $^5D_1\rightarrow{}^7F_J$ emission intensity.

Upon excitation close to the $^6G_{7/2}$ level, quantum cutting through a two step-energy transfer can take place.[19] In the first step, cross relaxation Gd^{3+} (^6G_J), Eu^{3+} ($^7F_0$) / Gd^{3+} (^6P_J), Eu^{3+} ($^5D_0$)

yields one photon, this step will feed only the $^5D_0$ level. In the second step, energy is transferred from the ^6P_J level of Gd^{3+} to a higher energy level of Eu^{3+}, yielding a normal branching ratio for the different ^5D_J emission bands. When excited at 275 nm (^6I_J), a single energy transfer step to Eu^{3+} occurs with normal branching ratio for the different ^5D_J emission bands. As a result, if quantum cutting through a two step-energy transfer process happens, significant increase in the emission intensity from $^5D_0$ will be observed. This is the case for our samples confirming the occurrence of quantum cutting. The $^5D_0/^5D_{0,1,2}$ ratios were calculated both for the excitations at 210 nm and 275 nm and the quantum efficiency of 115, 121 and 118 % are achieved for β-$NaGdF_4$respectively doped 1, 5 and 10% Eu^{3+}. These values are lower than that found for β-$NaGdF_4$: 2 mol% Eu^{3+}nanorods [20] in which the quantum efficiency reaches 187 %. Such a discrepancy can perhaps be explained by the absence of pure resonant excitation in the $^6G_{7/2}$ level, leading to some losses by multiphonon relaxations during the cross-relaxation step. VUV excitation using more adapted experimental set-up are planned to explore in more probing manner the quantum cutting process in our samples. Same considerations concern the Pr^{3+} doped β-$NaGdF_4$ for which a quantum-cutting was reported in β-$NaYF_4$:Pr^{3+}nanocrystals.[21] An emission spectrum under 210 nm excitation was recorded and depicted in **Figure 19**, showing, in addition to the $^6P_{7/2}\rightarrow{}^8S_{7/2}$ transition peaking at ~ 311 nm, a broad band, which is not observed in the case of β-$NaGdF_4$:Eu^{3+} and which can correspond to the Self-Trapped Emission (STE) as reported in the case of β-$NaYF_4$:Pr^{3+}nanocrystals.[21] Peaks with very low intensities, which nicely fit the positions of the emitting transitions related to Pr^{3+} ions as reported on Figure 13, are also observed (marked by a line on Figure 19). Observation of the $^6P_{7/2}\rightarrow{}^8S_{7/2}$ transition of Gd^{3+}under such excitation confirms that no energy transfer $Gd^{3+}\rightarrow Pr^{3+}$ occurs in β-$NaGdF_4$:Pr^{3+} NPs.

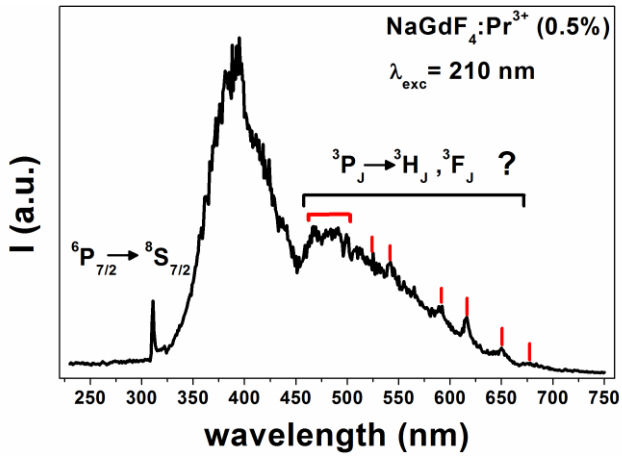

Figure 19 : Emission spectrum of β-$NaGdF_4$:Pr^{3+} (0.5 mol%) recorded at RT upon excitation at 210 nm.

Further experiments are planned to efficiently explore the quantum cutting phenomenon in β-$NaGdF_4$:Pr^{3+}.

Conclusion

We reported a very easy and tunable strategy for rapid fabrication of hexagonal phase β-$NaGdF_4$:Ln^{3+} (Ln=Eu or Pr) nanorods at low temperature for the first time, leading to nanorods of around 140 nm in the length characterized by a highly uniform distribution. Experimental results indicate that the Eu^{3+}or Pr^{3+}doping rates have no effect on both crystalline phase and morphology of the β-$NaGdF_4$ NPs. This new synthesis process could be applied to the whole lanthanide series. The optical properties of Eu^{3+} or Pr^{3+}doped β-$NaGdF_4$ were then deeply studied as a function of the luminescent active ions content and wavelength excitation. The strongest luminescence was observed for β-$NaGdF_4$: 20%Eu^{3+} and β-$NaGdF_4$: 0.5%Pr^{3+}. The measured decay times of the luminescence arising from the main emitting levels of Eu^{3+} or Pr^{3+} under near VUV, UV or visible excitations, show characteristic radiative de-excitations, the time constants of which are quite close to that found in bulk materials. Quantum cutting by down conversion process between Gd^{3+} and Eu^{3+} was also evidenced upon near VUV excitation. STE emission is also observed in the case of Pr^{3+} doped β-$NaGdF_4$.

The analysis of optical intensities and comparison with measured lifetimes was performed by means of the Judd–Ofelt theory based on luminescence spectra. The observed emission bands

$^5D_0 \rightarrow {}^7F_1$and $^5D_0 \rightarrow {}^7F_2$ of Eu^{3+} are well-resolved, which enabled the determination of the Ω_2 and Ω_4 intensity parameter values. A low value of asymmetry parameter Ω_2 was obtained, which indicates a relatively high symmetry at the Eu^{3+} sites. Including branching ratio measurements into the analysis allows the Judd–Ofelt parameters to be reliably calculated from emission spectra of Pr^{3+} ions embedded in β-$NaGdF_4$. Ω_2 parameter was found to be strongly dependent on the Pr^{3+} concentration and was used to explain the difference in the emission shapes of Pr^{3+} emission depending on its concentration in β-$NaGdF_4$.

ASSOCIATED CONTENT

Supporting Information.

The following files are available free of charge.

-**SI-1**: Detailed procedure of the calculation of JO parameters for Eu^{3+}-doped β-$NaGdF_4$ (PDF)

- **SI-**2: Detailed procedure of the calculation of JO parameters for Pr^{3+}-doped β-$NaGdF_4$ (PDF)

AUTHOR INFORMATION

Corresponding Authors

audrey.potdevin@sigma-clermont.fr or rachid.mahiou@uca.fr

Author Contributions

The manuscript was written through contributions of all authors.

Funding Sources

This research was performed as a part of joint PHC-Tassili, Algeria-France R&D Project (project N° 16MDU959) supported by Campus France (project N° 35079VB). Y. Cheroura

and Z. Smara are also grateful to the USTHB (Algeria) for providing a training grant under the faculty of physics program 2018-2019.

ACKNOWLEDGMENTS

Y. Cheroura and Z. Smara are grateful to the USTHB (Algeria) for providing a training grant under the faculty of physics program 2018-2019 and for the International Relations Department of UCA (France) for their facilities supports. We thank Christelle Blavignac (CICS, UCA) for TEM observations.

References

[1] S. Gai, C. Li, P. Yang, J. Lin, Chem. Rev., 114 (2014) 2343-2389, DOI: 10.1021/cr4001594.
[2] Z.-L. Wang, J.H. Hao, H.L.W. Chan, J. Mater. Chem., 20 (2010) 3178-3185, DOI: 10.1039/B924448D.
[3] X. Chen, J. Vanacken, J. Han, Z. Zhong, L. Li, Y. Han, Y. Liu, V.V. Moshchalkov, J. Appl. Phys., 121 (2017) 163103, DOI: 10.1063/1.4982349.
[4] A. Herrmann, M. Tylkowski, C. Bocker, C. Rüssel, Chem. Mater., 25 (2013) 2878-2884, DOI: 10.1021/cm401454y.
[5] P. Ghosh, A.-V. Mudring, Nanoscale, 8 (2016) 8160-8169, DOI: 10.1039/C6NR00172F.
[6] G. Tessitore, A.-V. Mudring, K.W. Krämer, J. Lumin., 189 (2017) 91-98, DOI: 10.1016/j.jlumin.2017.03.021.
[7] C. Cheng, Y. Xu, S. Liu, Y. Liu, X. Wang, J. Wang, G. De, J. Mater. Chem. C, (2019), DOI: 10.1039/C9TC01323G.
[8] P. Lei, P. Zhang, S. Yao, S. Song, L. Dong, X. Xu, X. Liu, K. Du, J. Feng, H. Zhang, ACS Appl. Mater. Interfaces, 8 (2016) 27490-27497, DOI: 10.1021/acsami.6b08335.
[9] J. Ryu, H.-Y. Park, K. Kim, H. Kim, J.H. Yoo, M. Kang, K. Im, R. Grailhe, R. Song, J. Phys. Chem. B, 114 (2010) 21077-21082, DOI: 10.1021/jp107725r.
[10] E. Hemmer, M. Quintanilla, F. Légaré, F. Vetrone, Chem. Mater., 27 (2015) 235-244, DOI: 10.1021/cm503799f.
[11] N. Martin, P. Boutinaud, R. Mahiou, J.-C. Cousseins, M. Bouderbala, J. Mater. Chem., 9 (1999) 125-128, DOI: 10.1039/A804472D.
[12] M. Banski, A. Podhorodecki, J. Misiewicz, M. Afzaal, A.L. Abdelhady, P. O'Brien, J. Mater. Chem. C, 1 (2013) 801-807, DOI: 10.1039/C2TC00132B.
[13] R. Gao, L. Sun, L. Li, T. Pan, L. Fu, X.-C. Ai, J.-P. Zhang, New J. Chem., 43 (2019) 7198-7201, DOI: 10.1039/C9NJ01226E.
[14] G. Tessitore, A.-V. Mudring, K.W. Krämer, New J. Chem., 42 (2018) 237-245, DOI: 10.1039/C7NJ03242K.
[15] P. Du, L. Luo, X. Huang, J.S. Yu, J. Colloid Interface Sci., 514 (2018) 172-181, DOI: 10.1016/j.jcis.2017.12.027.
[16] J.W. Chung, J.Y. Park, H.K. Yang, J. Lumin., 211 (2019) 176-182, DOI: 10.1016/j.jlumin.2019.03.010.
[17] P. Lei, R. An, S. Yao, Q. Wang, L. Dong, X. Xu, K. Du, J. Feng, H. Zhang, Adv. Mater., 29 (2017) 1700505, DOI: 10.1002/adma.201700505.
[18] M.J. Weber, T.E. Varitimos, B.H. Matsinger, Phys. Rev. B, 8 (1973) 47-53, DOI: 10.1103/PhysRevB.8.47.

[19] R.T. Wegh, H. Donker, K.D. Oskam, A. Meijerink, J. Lumin., 82 (1999) 93-104, DOI: 10.1016/S0022-2313(99)00042-3.
[20] P. Ghosh, S. Tang, A.-V. Mudring, J. Mater. Chem., 21 (2011) 8640-8644, DOI: 10.1039/C1JM10728C.
[21] M.A. Gusowski, H.C. Swart, L.S. Karlsson, M. Trzebiatowska-Gusowska, Nanoscale, 4 (2012) 541-546, DOI: 10.1039/C1NR11249J.
[22] T. Hirai, H. Yoshida, S. Sakuragi, S. Hashimoto, N. Ohno, Jpn. J. Appl. Phys., 46 (2007) 660-663, DOI: 10.1143/jjap.46.660.
[23] J. Xu, S. Gai, P.a. Ma, Y. Dai, G. Yang, F. He, P. Yang, J. Mater. Chem. B, 2 (2014) 1791-1801, DOI: 10.1039/C3TB21465F.
[24] J. Yang, J. Dong, R. Wu, H. Wu, H. Song, S. Gan, L. Zou, Dalton Trans., 47 (2018) 9795-9803, DOI: 10.1039/C8DT01991F.
[25] X. Jiang, Y. Wang, T. Herricks, Y. Xia, J. Mater. Chem., 14 (2004) 695-703, DOI: 10.1039/B313938G.
[26] Q. Zhao, B. Shao, W. Lü, W. Lv, M. Jiao, L. Zhao, H. You, Dalton Trans., 44 (2015) 3745-3752, DOI: 10.1039/C4DT03619K.
[27] W. Zhang, Y. Shen, M. Liu, P. Gao, H. Pu, L. Fan, R. Jiang, Z. Liu, F. Shi, H. Lu, ACS Appl. Mater. Interfaces, 9 (2017) 39985-39993, DOI: 10.1021/acsami.7b11295.
[28] J.J. Velázquez, R. Balda, J. Fernández, G. Gorni, L. Pascual, G. Chen, M. Sundararajan, A. Durán, M.J. Pascual, J. Lumin., 193 (2018) 61-69, DOI: 10.1016/j.jlumin.2017.07.034.
[29] Y.Q. Jia, J. Solid State Chem., 95 (1991) 184-187, DOI: 10.1016/0022-4596(91)90388-X.
[30] A.I. Becerro, D. González-Mancebo, E. Cantelar, F. Cussó, G. Stepien, J.M. de la Fuente, M. Ocaña, Langmuir, 32 (2016) 411-420, DOI: 10.1021/acs.langmuir.5b03837.
[31] K. Vukovic, M. Medic, M. Sekulic, M. Dramicanin, Adv. Cond. Matter Phys., 2015 (2015) 7, DOI: 10.1155/2015/736517.
[32] L. Đačanin, S.R. Lukić, D.M. Petrović, M. Nikolić, M.D. Dramićanin, Physica B, 406 (2011) 2319-2322, DOI: 10.1016/j.physb.2011.03.068.
[33] P. Ghosh, R.K. Sharma, Y.N. Chouryal, A.-V. Mudring, RSC Adv., 7 (2017) 33467-33476, DOI: 10.1039/C7RA06741K.
[34] A. Bednarkiewicz, A. Mech, M. Karbowiak, W. Stręk, J. Lumin., 114 (2005) 247-254, DOI: 10.1016/j.jlumin.2005.01.005.
[35] F. Hund, Z. Anorg. Chem., 261 (1950) 106-115, DOI: 10.1002/zaac.19502610110.
[36] H.S. Kiliaan, J.F.A.K. Kotte, G. Blasse, Chem. Phys. Lett., 133 (1987) 425-428, DOI: 10.1016/0009-2614(87)87095-1.
[37] P. Ptacek, H. Schäfer, K. Kömpe, M. Haase, Adv. Funct. Mater., 17 (2007) 3843-3848, DOI: 10.1002/adfm.200600974.
[38] D. Zakaria, R. Mahiou, D. Avignant, M. Zahir, J. Alloys Compd., 257 (1997) 65-68, DOI: 10.1016/S0925-8388(97)00016-9.
[39] D. Tu, Y. Liu, H. Zhu, R. Li, L. Liu, X. Chen, Angew. Chem., 125 (2013) 1166-1171, DOI: 10.1002/ange.201208218.
[40] P. Boutinaud, R. Mahiou, N. Martin, M. Malinowski, J. Lumin., 72-74 (1997) 809-811, DOI: 10.1016/S0022-2313(96)00173-1.
[41] W. Ryba-Romanowski, S. Gołvab, G. Dominiak-Dzik, P. Solarz, Appl. Phys. A, 74 (2002) 581-586, DOI: 10.1007/s003390100917.
[42] M. Inokuti, F. Hirayama, J. Phys. Chem., 43 (1965) 1978-1989, DOI: 10.1063/1.1697063.
[43] M. Yokota, O. Tanimoto, J. Phys. Soc. Jpn., 22 (1967) 779-784, DOI: 10.1143/JPSJ.22.779.
[44] M.N. Berberan-Santos, E.N. Bodunov, B. Valeur, Chem. Phys., 317 (2005) 57-62, DOI: 10.1016/j.chemphys.2005.05.026.
[45] R. Mahiou, J.C. Cousseins, M.T. Fournier, J. Chim. Phys., 85 (1988) 769-773, DOI: 10.1051/jcp/1988850769
[46] B. Tian, B. Chen, Y. Tian, X. Li, J. Zhang, J. Sun, H. Zhong, L. Cheng, S. Fu, H. Zhong, Y. Wang, X. Zhang, H. Xia, R. Hua, J. Mater. Chem. C, 1 (2013) 2338-2344, DOI: 10.1039/C3TC00915G.

[47] Y. Tian, B. Chen, R. Hua, J. Sun, L. Cheng, H. Zhong, X. Li, J. Zhang, Y. Zheng, T. Yu, L. Huang, H. Yu, J. Appl. Phys., 109 (2011) 053511, DOI: 10.1063/1.3551584.
[48] Y. Zhang, B. Chen, S. Xu, X. Li, J. Zhang, J. Sun, X. Zhang, H. Xia, R. Hua, Phys. Chem. Chem. Phys., 20 (2018) 15876-15883, DOI: 10.1039/C8CP02317D.
[49] N. Martin, P. Boutinaud, M. Malinowski, R. Mahiou, J.C. Cousseins, J. Alloys Compd., 275-277 (1998) 304-306, DOI: 10.1016/S0925-8388(98)00323-5.
[50] M. Malinowski, M.F. Joubert, B. Jacquier, J. Lumin., 60-61 (1994) 179-182, DOI: 10.1016/0022-2313(94)90124-4.
[51] H. Chen, R. Lian, M. Yin, L. Lou, W. Zhang, S. Xia, J.-C. Krupa, J. Phys.: Condens. Matter, 13 (2001) 1151-1158, DOI: 10.1088/0953-8984/13/5/328.
[52] R. Naik, S.C. Prashantha, H. Nagabhushana, S.C. Sharma, D.M. Jnaneshwara, K.S. Ananthraju, H.P. Nagaswarupa, H.B. Premkumar, M. Chandrasekhar, AIP Conf. Proc., 1731 (2016) 050034, DOI: 10.1063/1.4947688.

Supporting information SI-1

The oscillator strength between two states 4f; SLJ and 4f; S'L'J' of rare-earth ions can be calculated in the Judd–Ofelt theory for both the electric dipole ED and magnetic dipole MD contributions [1]

$$f(J;J') = \frac{8\pi^2 m\bar{\nu}}{3(2J+1)he^2} S(J;J') \quad (1)$$

where$S(J;J')$ represent the electric $S_{ed}(J;J')$ or magnetic $S_{md}(J;J')$ dipole strengths [1]:

$$S_{ed}(J;J') = e^2 \sum_{teven} \Omega_t \left|\langle \Psi J \left| U^{(t)} \right| \Psi J' \rangle\right|^2 \quad (2)$$

$$S_{md}(J;J') = \mu_B^2 \left|\langle \Psi J \left| \vec{L} + 2\vec{S} \right| \Psi J' \rangle\right|^2 \text{ with } \mu_B^2 = \frac{e\hbar}{2mc} \quad (3)$$

Where $\bar{\nu}$ is the average transition frequency, h denotes Planck constant (6.626×10^{-34}J·s), m was the electron masse, c the velocity of light, n is the refractive index, $2J + 1$ is the degeneracy of the initial state, , $\Omega_t$are the Judd-Ofelt parameters, and$\langle \Psi J \| U(\lambda) \| \Psi J' \rangle$terms are the double reduced matrix elements of unit tensor operators whose values are independent of the local environment of the ion.

The oscillator strength can be also expressed in terms of integrated emission cross sections $\sigma(\nu)$ by the relationship [1]:

$$f(J;J') = \frac{mcn^2}{\pi e^2 \chi} \int \sigma(\nu) d\nu \quad (4)$$

$\chi$was the local field correction factor$\chi_{ed} = \frac{n(n^2+2)^2}{9}$for electric dipole emission and $\chi_{md} = n^3$ for magnetic dipole emission.

From (1) and (4) we can write

$$\frac{8\pi^2 m\bar{\nu}}{3(2J+1)he^2} S(J;J') = \frac{mcn^2}{\pi e^2 \chi} \int \sigma(\nu) d\nu \ (5)$$

For the Eu^{3+} ions The $^5D_0 \rightarrow {}^7F_1$ transition is magnetic dipole in nature, its intensity is largely independent of the environment ,this transition can be considered as a reference for all transitions originating from the $^5D_0$excited state

$$\frac{8\pi^2 m\bar{\nu}}{3(2J+1)he^2} S_{md}(5D_0; 7F_1) = \frac{mcn^2}{\pi e^2 \chi} \int \sigma_1(\nu) d\nu \quad (6)$$

On the other hand, the $^5D_0 \rightarrow {}^7F_{2,4,6}$ are induced electric dipole transitions, We can observe from Table 1 and Eq.(2) that each electric dipolar $^5D_0 \rightarrow {}^7F_{2,4,6}$transition depends only on one squared reduced matrix element.

$$\frac{8\pi^2 m\bar{\nu}}{3(2J+1)he^2} S_{ed}(5D_0; 7F_t) = \frac{mcn^2}{\pi e^2 \chi} \int \sigma_t(\nu) d\nu \quad \text{Where} \quad S_{ed}(5D_0; 7F_t) = e^2 \Omega_t \left|\langle \Psi J | U^{(t)} | \Psi J' \rangle\right|^2 \quad (7)$$

This unique feature for the Eu^{3+} ion (non diagonal elements of the $\left|\langle \Psi J | U^{(t)} | \Psi J' \rangle\right|^2$ matrix have zero values) facilitates the determination of JO parameters from the emission spectra. The experimental intensity Ω_t can be calculated (using eq. 6,7) from the ratio of the intensity of the $^5D_0 \rightarrow {}^7F_t$ (t=2,4,6) transitions $\int \sigma_t(\nu) d\nu$, to the intensity of the $^5D_0 \rightarrow {}^7F_1$ transition $\int \sigma_t(\nu) d\nu$ as follows:

$$\Omega_t = \frac{S_{md} \nu_1}{e^2 \nu_t} \frac{9n^3}{n(n^2+2)^2} \frac{1}{\left|\langle \Psi J | U^{(t)} | \Psi J' \rangle\right|^2} \frac{\int \sigma_t(\nu) d\nu}{\int \sigma_1(\nu) d\nu} \quad (8)$$

Then, probabilities of each spontaneous emission (radiative rates) can be obtained using calculated $\Omega_t$parameters from **[1]:**

$$A(J; J') = \frac{64\pi^4 \bar{\nu}^3 \chi}{3(2J+1)hc^3} S(J; J') \quad (9)$$

And the radiative life time of an excited state j ($^5D_0$) is simply

$$\frac{1}{\tau_j} = \sum_{j'} A j j'$$

where the summation is over electric and magnetic dipole transitions to all terminal states $7F_{j'}$.

Table 1.Squared reduced matrix elements used for the calculation of dipole strengths of the ED transitions in the emission spectra of Eu^{3+}, taken from **[5].**

$^5D_0 \rightarrow$	$\left\|\langle \Psi J \| U^{(2)} \| \Psi J' \rangle\right\|^2$	$\left\|\langle \Psi J \| U^{(4)} \| \Psi J' \rangle\right\|^2$	$\left\|\langle \Psi J \| U^{(6)} \| \Psi J' \rangle\right\|^2$
$^7F_2$	0.0032	0	0
$^7F_4$	0	0.0023	0
$^7F_6$	0	0	0.0002

Results

Magnetic dipole strength $S_{md}(5D_0; 7F_1)$

$$S_{md}(5D_0; 7F_1) = \mu_B^2 \left|\langle 5D_0 \left|\vec{L} + 2\vec{S}\right| 7F_1\rangle\right|^2$$

Where the matrix element $\langle 5D_0 \left|\vec{L} + 2\vec{S}\right| 7F_1\rangle$ can be calculated the relationship [2]

$$\langle 5D_0 \left|\vec{L} + 2\vec{S}\right| 7F_1\rangle = 0.109329$$

$$S_{md}(5D_0; 7F_1) = 1{,}044 \,.\, 10^{-64}\ C^2m^2$$

Judd-Ofelt parameters Ω_t

Ω_2

Ω_2 was calculated using the equation (8) where :

- the refractive index of β-$NaGdF_4$ was measured by Thoma *et al.*[3]. The hexagonal crystal $NaGdF_4$ is birefringent, with ordinary and extraordinary refractive indices $n_0 = 1.507$ and $n_e = 1.483$ respectively. The birefringence is small with $\Delta n = -0.24$, and hence an average index $\bar{n} = \frac{1}{3}(2n_0 + n_e) = 1.499$[3].Taking into account that refractive index is wavelength-dependent, taking the constant value into calculation introduces small error into obtained values since the refractive index changes are small over the wavelength region of interest (590–800 nm). This simplification is justified for the sake of comparison of JO parameters between samples since this cannot change observed trends. Also, this error is smaller than rms error for the JO procedure [4].

- the average transition $5D_0 \rightarrow 7F_2$ frequency $\bar{\nu}_2 = 16260 cm^{-1}$

- the average transition $5D_0 \rightarrow 7F_1$ frequency $\bar{\nu}_1 = 16920 cm^{-1}$

- the ratio of the intensity of the $5D_0 \rightarrow 7F_2$ transition to the intensity of $5D_0 \rightarrow 7F_1$transition $\frac{\int \sigma_2(\nu) d\nu}{\int \sigma_1(\nu) d\nu} = 1.6$

- the squared reduced matrix element $\left|\langle \Psi J \left|U^{(2)}\right| \Psi J' \rangle\right|^2 = 0.0032$ [5]

$$\Omega_2 = 2.333 \,.\, 10^{-20} cm^2$$

Ω_4

Ω_4 was calculated using the equation (8) where :

- the average transition $5D_0 \rightarrow 7F_4$ frequency $\bar{\nu}_2 = 14368 cm^{-1}$

- the average transition $5D_0 \rightarrow 7F_1$ frequency $\bar{\nu}_1 = 16920 cm^{-1}$

- the ratio of the intensity of the $5D_0 \rightarrow 7F_4$ transition to the intensity of $5D_0 \rightarrow 7F_1$transition $\frac{\int \sigma_4(\nu)d\nu}{\int \sigma_1(\nu)d\nu} = 0.42$

- the squared reduced matrix element $\left|\langle \Psi J \left| U^{(2)} \right| \Psi J' \rangle\right|^2 = 0.0023$ [5]

$$\Omega_4 = 9.897 \,.\, 10^{-21} cm^2$$

The Ω_6 intensity parameter was not determined because the $5D_0 \rightarrow 7F_6$ transition could not be experimentally detected.

Electric dipole strengths

$$\mathrm{S_{ed}}(5\mathrm{D}_0; 7\mathrm{F}_2) = e^2\Omega_2\left|\langle \Psi J \left| U^{(2)} \right| \Psi J' \rangle\right|^2 = 1.938 \,.\, 10^{-64}\ C^2m^2$$

$$\mathrm{S_{ed}}(5\mathrm{D}_0; 7\mathrm{F}_4) = e^2\Omega_4\left|\langle \Psi J \left| U^{(4)} \right| \Psi J' \rangle\right|^2 = 5.827 \,.\, 10^{-65}\ C^2m^2$$

Probabilities of spontaneous emission

$$A(J;J') = \frac{64\pi^4\bar{\nu}^3\chi}{3(2J+1)hc^3}S(J;J')$$

$$\mathrm{A}(5\mathrm{D}_0; 7\mathrm{F}_1) = 48.030\ s^{-1}$$

$$\mathrm{A}(5\mathrm{D}_0; 7\mathrm{F}_2) = 70.570\ s^{-1}$$

$$\mathrm{A}(5\mathrm{D}_0; 7\mathrm{F}_4) = 14.640\ s^{-1}$$

$$\frac{1}{\tau_i} = \sum_j Aij$$

$$\tau_{5D_0} = 7.5\ ms$$

This value which depends on the experimental set-up is obtained with an uncertainty of 5%.

References

[1] Weber,M. J.; Varitimos,T. E.; Matsinger,B. H. Phys. Rev. B 1973, 8, 47-53.

[2]Carnall,W. T.; Fields,P. R.; WybourneB. G. J. Chem. Phys. 1965, 42, 3797-3805.

[3]Thoma,R.E.; Insley,H.; Hebert,G.M. Inorg. Chem. 1966, 1222-1229.

[4]Dacanin,Lj.; Lukic´,S. R.; Petrovic´,D.M.; Nikolic´,M.; Dramicanin, M.D. Physica B 2011, 406, 2319–2322.

[5]Carnall,W.T.; Fields,P.R.; Rajnak,K. J. Chem. Phys. 1968, 49, 4450-4455.

Supporting information SI-2

From the experimental luminescence decay curves of the $^3P_0$-$^3H_4$ transition of Pr^{3+} ion, we calculated the radiative life time values of the $^3P_0$ state for the pure hexagonal $NaGdF_4$:Pr^{3+} (0.1, 0.5, 1%) samples

Then, the total radiative decay rate (probability of spontaneous emission) of the $^3P_0$ state can be obtained using

$$A_{3P_0} = \frac{1}{\tau_{3P_0}}$$

For a particular transition, the emission intensity I_i can be considered as proportional to the area under the emission curve for that transition. Also, the intensity will be proportional to the radiative decay rate of the transition **[1]**:

$$\mathrm{A_2}(3\mathrm{P_0};3\mathrm{F_2}) = \frac{I_2}{I_T}A_{3P_0}$$

$$\mathrm{A_4}(3\mathrm{P_0};3\mathrm{H_4}) = \frac{I_4}{I_T}A_{3P_0}$$

$$\mathrm{A_6}(3\mathrm{P_0};3\mathrm{H_6}) = \frac{I_6}{I_T}A_{3P_0}$$

Where I_i is the emission intensity of the transition $^3P_0 \rightarrow$ i, and $I_T$represent the sum of intensities of all $^3P_0 \rightarrow$ i transitions $I_T = \sum_i I_i$

Or, the probability of each spontaneous emission is related to the oscillator strengths by

$$A(J;J') = \frac{64\pi^4\bar{\nu}^3\chi}{3(2J+1)hc^3}S(J;J')$$

For the Pr^{3+} ions, the $^3P_0 \rightarrow {}^3F_2$ and $^3P_0 \rightarrow {}^3H_{4,6}$ are induced electric dipole transitions, we can write:

$$\mathrm{A_t}(J;J') = \frac{64\pi^4\bar{\nu}^3\chi}{3(2J+1)hc^3}S_{ed}(J;J') = \frac{64\pi^4\bar{\nu}^3\chi}{3(2J+1)hc^3}\left[e^2\sum_{teven}\Omega_t\left|\langle\Psi J\left|U^{(t)}\right|\Psi J'\rangle\right|^2\right]$$

The experimental intensity Ω_t can be calculated as follows:

$$\Omega_t = \frac{3(2J+1)hc^3}{64\pi^4\bar{\nu}^3\chi e^2}\frac{\mathrm{A_t}(J;J')}{|\langle\Psi J|U^{(t)}|\Psi J'\rangle|^2}$$

Table 1. Squared reduced matrix elements of Pr^{3+} **[2]**

$^3P_0 \rightarrow$	$\left\|\langle\Psi J\left\|U^{(2)}\right\|\Psi J'\rangle\right\|^2$	$\left\|\langle\Psi J\left\|U^{(4)}\right\|\Psi J'\rangle\right\|^2$	$\left\|\langle\Psi J\left\|U^{(6)}\right\|\Psi J'\rangle\right\|^2$
$^3F_2$	0.2951	0	0
$^3H_4$	0	0.1719	0
$^3H_6$	0	0	0.0726

Results

Total radiative decay rate of the $^3P_0$ state

Pr^{3+} conc. (mol %)	τ_{3P_0}(μs)	$A_{3P_0}(s^{-1})$
0.1	31.5	31725.9
0.5	36.2	27593.8
1	35.1	28481.9

Probabilities of spontaneous emission

Pr^{3+} conc. (mol %)	$A_2(s^{-1})$	$A_4(s^{-1})$	$A_6(s^{-1})$
0.1	4124.4	13007.6	10152.3
0.5	3035.3	14072.9	7174.4
1	3133.0	14525.8	7405.3

Judd-Ofelt parameters Ω_t

Pr^{3+} conc. (mol %)	Ω_2 $(10^{-20}cm^2)$	$\Omega_4(10^{-20}cm^2)$	$\Omega_6(10^{-20}cm^2)$
0.1	5.25	0.12	0.44
0.5	3.73	0.13	0.31
1	3.85	0.13	0.44

References

[1]Naik, R.; Prashantha, S.C.; Nagabhushana, H.; Sharma, S.C.; Jnaneshwara, D.M.; Ananthraju, K.S.; Nagaswarupa, H.P.; Premkumar, H.B.; Chandrasekhar, M.DAE Solid State Physics Symposium 2015, 050034, 1-3.

[2]Babu, P.; Jayasankar, C.K.Physica B2001, 301, 326-340.